Int. J. Electrochem. Sci., 17 **(2022)** Article Number: 220322, doi: 10.20964/2022.03.25

International Journal of
ELECTROCHEMICAL
SCIENCE
www.electrochemsci.org

Improved visible light photocatalytic activity of Fe, N co-doped TiO_2 for degradation of o-chlorophenol in water

Hengbo Liu

College of Environmental Science and Engineering, Nankai University, TianJin 300350, China
E-mail: 2120210685@mail.nankai.edu.cn

Received: 17 November 2021 / *Accepted:* 5 January 2022 / *Published:* 2 February 2022

A nanostructured photocatalyst based on Fe, N co-doped TiO_2 (Fe_y + N_x/TiO_2; y = 0.5, 1, 2 and 3 %, and x = 2, 5, 10 and 13 %) was synthesized using the sol-gel method and applied for degradation of o-CP in water. The XRD, SEM analyses of prepared photocatalysts indicted the successful synthesis and doping of TiO_2 with Fe and N. Results of an EIS study illustrated that the doping process in Fe_y + N_x/TiO_2 decreased the charge transfer resistance and increased the carrier transfer rate between sample and electrolyte. UV–vis absorption spectra revealed that the optical band gap of pure TiO_2, Fe_2/TiO_2, N_{10}/TiO_2, and Fe_2+N_{10}/TiO_2 was obtained at 3.07, 2.98, 2.77 and 2.65 eV, respectively, indicating the doping leads to narrowing of the optical band gap and red-shifting of absorption towards the visible-light region. Photodegradation studies of Fe_y+N_x/TiO_2 showed that Fe_2+N_{10}/TiO_2 had the optimal content of Fe and N dopants for fast degradation of o-CP aqueous solution. The complete removal of 5, 10, 50 and 100 mg/l of o-CP was obtained after 120, 200, 255 and 360 minutes of simulated sunlight irradiation, respectively. Comparison of these results with photocatalytic performance of reported systems in the literature showed the effective performance of the prepared photocatalyst for photodegradation of o-CP under simulated sunlight because of the synergistic effect of both Fe and N in the Fe_2+N_{10}/TiO_2 nanoparticles that led to a decrease in the recombination rate of photogenerated carries and a narrowing band gap.

Keywords: Photocatalyst activity; Fe, N co-doped TiO_2 nanoparticles; Photodegradation; O-chlorophenol

1. INTRODUCTION

Chlorophenols are a major group of organochlorinated compounds of phenol that contain one or more covalently bonded chlorine atoms that are synthesized by treating phenol with chlorine and by hydrolysis of polychlorobenzenes [1, 2]. Most applications of chlorophenols are based on controlling bacteria, fungi, insects, and weeds [3, 4]. These toxicant compounds are persistent and recalcitrant to biodegradation, accordingly are widely spread in the environment [5]. Consequently, these

organochlorinated compounds exert high toxicity, mutagenicity, genotoxicity and carcinogenicity, and have the potential to change histopathological in humans and animals [6, 7]. Thermal and chemical degradation of chlorophenols can result in the formation of more toxic intermediates and harmful substances which on consumption cause serious health problems [8, 9]. Chlorophenol exposure affects the nervous system and reports have shown that workers who were exposed to high levels of chlorophenols experienced tremors, convulsions, and central nervous system depression [10-12].

Among these organochlorinated compounds, 2-Chlorophenol or ortho-chlorophenol (o-CP, 2-Hydroxychlorobenzene) as an organic compound is an isomeric monochloride derivative of phenol [13-15]. It belongs to a class of toxic organic compounds that are used as an intermediate for the synthesis of pesticides, dyes, medicines, disinfectants, personal care formulations, degreasers, resins, wood preservatives, aroma compounds and other organic chemicals [16-18]. o-CP is also utilized as a solvent for the extraction of sulfur and nitrogen compounds from coal [19, 20]. Therefore, many studies have been focused on degradation of the o-CP from industrial wastewaters using the electro-Fenton process [21], contact glow discharges [22, 23], pulsed high voltage discharge [24], aerobic biodegradation [25] and photodegradation [26-32].

Among these degradation methods, photodegaradation using photocatalysts is a technique based on chemical reaction to absorb and oxidize chlorophenols that occurs under the joint action of light and the photocatalysts and photogeneration electrons and holes [33-35]. Using photocatalysts, degaradation possesses several advantages such as low cost, eco-friendly, and attractive efficiency. However, modification of photoctalysts is necessary to improve the degradation rate and reduce the recombination rate of photogenerated carriers. Therefore, this study was performed to improve the visible light photocatalytic activity of Fe, N co-doped TiO_2 for the degradation of o-CP in water.

2. EXPERIMENTAL

2.1. Fe–N co-doped TiO_2 photocatalyst preparation

A Fe–N co-doped TiO_2 ($Fe_y + N_x/TiO_2$; y = 0.5, 1, 2 and 3 %, and x = 2, 5, 10 and 13 %) catalyst was prepared using the sol-gel method [36, 37]. In a volume ratio of 2:1:1, a mixture of Fe(NO3)39H2O (98%, Merck, Germany), 1 M glacial acetic acid (99%, Sigma-Aldrich), and 1 M nitric acid (99.5%, Sigma-Aldrich) was prepared, and titanium isopropoxide (97%, Merck, Germany) was added. Then, the 30% Arabic gum (Sigma-Aldrich) aqueous solution was separately prepared and stirred for 20 minutes at 55 °C. After cooling the Arabic gum aqueous solution, it along with the ammonium chloride (99.998%, Sigma-Aldrich) was added to the prepared mixture and the final mixture was stirred for 9 hours at room temperature. After that, the mixture was transferred to oven and dried at 110 °C, and subsequently calcined at 500 °C for 3 hours. To prepare $Fe_y + N_x/TiO_2$, the volume of 1 M nitric acid as an N source in photocatalysts was adjusted to obtain 2, 5, 10, and 13%, and the volume of $Fe(NO_3)_{39}H_2O$ as an Fe source in photocatalysts was adjusted to obtain 0.5, 1, 2, and 3%, which were added to titanium isopropoxide as the Ti source. These specimens for undoped sample referred as TiO_2, and for N doped TiO_2 are referred to as N_x/TiO_2 (N_2/TiO_2, N_5/TiO_2, N_{10}/TiO_2

and N_{13}/TiO_2,), for Fe doped TiO_2 are referred to as Fe_y/TiO_2 ($Fe_{0.5}/TiO_2$, Fe_1/TiO_2, Fe_2/TiO_2 and Fe_3/TiO_2), and co-doped photocatalysts are referred to as $Fe_y + N_x/TiO_2$ ($Fe_{0.5} + N_{10}/TiO_2$, $Fe_1 + N_{10}/TiO_2$, $Fe_2 + N_{10}/TiO_2$, $Fe_3 + N_{10}/TiO_2$, $Fe_2 + N_2/TiO_2$, $Fe_2 + N_5/TiO_2$ and $Fe_2 + N_{13}/TiO_2$).

2.2. Characterization

XRD techniques were used for the crystallographic analyses by an X-ray diffractometer (D8 advance; Bruker AXS, Madison, WI). The morphological analyses of nanostructures were performed on a scanning electron microscope (SEM, Zeiss ULTRA plus with Charge Compensation). The UV–vis absorption spectra of samoles were analyzed in the range of 200–800 nm by the UV–vis spectrometer (HITACHI, U-3900H, Tokyo, Japan). The (EIS) measurements were carried out using the Autolab system (PGSTAT 30, Ecochemie, Netherlands) with a three-electrode cell configuration consisting of a modified GCE as working electrode (electrode surface of $1cm^2$), a platinum wire electrode as counter, and a saturated Ag/AgCl electrode as a reference, at a frequency range from 10^{-1} Hz to 10^5 Hz and an applied 5 mV sine wave ac voltage in 0.5 M Na_2SO_4 (≥99%, Merck, Germany) aqueous solution. For modification of the GCE surface, the 10 µl of Nafion (Sigma-Aldrich) was dropped on clean GCE surface, and 10 mg/ml of dispersed pure or doped TiO_2 was dropped on the GCE surface. Then, the electrode surfaces were dried under an IR lamp to obtain the TiO_2 and $Fe_y + N_x/TiO_2$ modified GCE [38].

2.3. Photocatalytic degradation studies

The photocatalysis analysis of pure and doped TiO_2 under irradiation simulated sunlight (a 150 W/m 2 xenon lamp) was conducted in a 150 mL glass bottle for degradation of 100 ml of 5 mg/l to 100 mg/l of o-CP (99%, SigmaAldrich) aqueous solution. The simulated sunlight source was located around 8 cm from one side of the bottle. Before the light irradiation, all samples and photocatalysts were kept in the dark for 2 hours to establish the absorption/desorption equilibrium. Photodegradation of o-CP was analyzed using UV–Vis spectroscopy (Hitachi U-3900H, Japan), and the evolution of the visible absorption spectrum was studied to determine the change of o-CP and degradation efficiency using the following equation:

$$\text{Degradation efficiency (\%)} = \frac{C_0 - C_t}{C_0} \times 100 = \frac{I_0 - I_t}{I_0} \times 100 \qquad (1)$$

where, C_0 and C_t (mg/L) are the initial amount of o-CP concentration, and the amount of o-CP concentration after light irradiation at time t (minute), respectively. I_0 and I are the absorbance of o-CP solution before and after light irradiation, respectively.

3. RESULTS AND DISCUSSION

3.1. XRD and SEM analyses

Figure 1 displays the XRD patterns of the powders of pure TiO_2, Fe_2/TiO_2, N_{10}/TiO_2, and Fe_2 + N_{10}/TiO_2. As observed, all XRD patterns of pure TiO_2 show the diffraction peaks corresponding to the anatase and rutile phases of TiO_2 according to JCPDS card No. 21-1272 and 21- 1276, respectively. In addition, no characteristic peak of impurities is found for doped TiO_2. As seen, the (200) and (211) planes of the rutile phase are eliminated after Fe-doping which implies that Fe-doping may lead to a transition from anatase to rutile [39, 40].

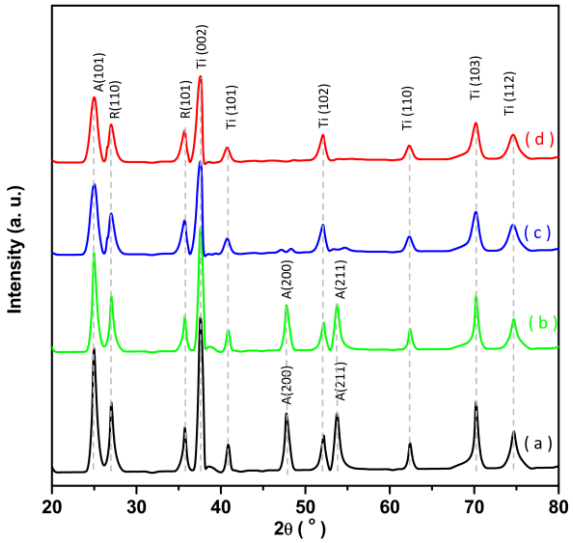

Figure 1. XRD patterns of the powders of (a) pure TiO_2, (b) N_{10}/TiO_2, (c) Fe_2/TiO_2 and (d) Fe_2 + N_{10}/TiO_2.

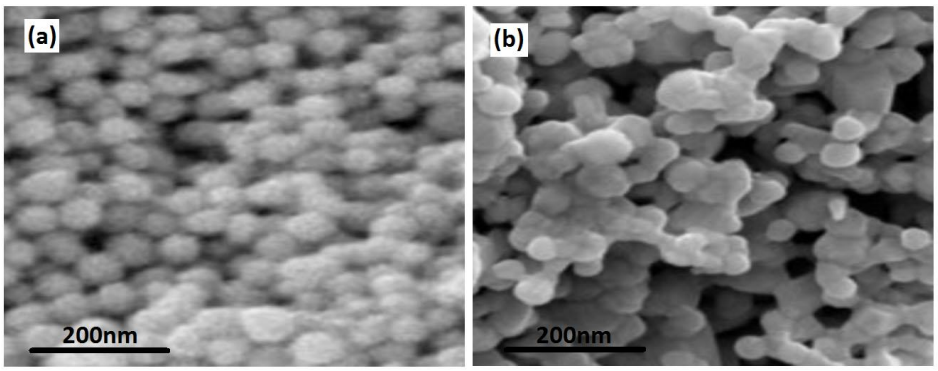

Figure 2. SEM images of the synthesized (a) pure TiO_2, (b) Fe_2 + N_{10}/TiO_2.

Figure 2 shows the SEM images of the synthesized pure TiO_2 and Fe_2 + N_{10}//TiO_2. As seen from the SEM image of Figure 2a, the sol–gel synthesized pure TiO_2 nanoparticles are spherical in shape and the average size of nanoparticles is 55nm. The SEM image of Figure 2b reveals that Fe_2+N_{10}/TiO_2 is also spherical in shape with an average size of 50nm, respectively, indicating that

doping with Fe and N elements will retard the growth of the nanoparticle sizes, and decrease the diameter of nanoparticles, which is in agreement with reports in [41, 42]. After the doping, the surfaces of TiO_2 nanoparticles changed from the smooth surface to one containing bulges on it. The XRD and SEM results indicated successful synthesis and doping of TiO_2 with Fe-N.

3.2. EIS analysis

Electrochemical properties of pure and doped TiO_2 samples were analyzed using the EIS technique to simulated sunlight, and related Nyquist curves are shown in Figure 3. It can be observed from Figure 3a that all of the samples show an incomplete semicircle, which is the characteristic of a capacitive system indicating non-ideal behavior [43], and the semicircle radius presents the charge transfer resistance at the liquid/solid interface. Therefore, the impedance data was fitted using an equivalent circuit in Figure 3b, which contained of two RC elements connected in series. The resistive and capacitive elements are directly related to individual charge transfer processes. As illustrated in Figure 3b, CPE stands for constant phase elements and Rs is the series resistance. Rsc is the charge transfer resistance inside the photocatalyst, and Rct corresponds to the charge transfer resistance at the photocatalyst/electrolyte interface [44]. The impedance of the CPE is given by:

$$Z_Q = Y_0^{-1} (j\omega)^{-n} \quad (0 \leq n \leq 1) \qquad (2)$$

Where Y0 is the admittance of an ideal capacitance, j is the imaginary number ($j^2 = -1$), ω is the signal frequency and n is an frequency power, ranging from 0-1 [45]. The Rct component defines the process of hole transportation from the electrode surface to the electrolyte [46]. The values of the circuit elements have been deduced and are displayed in Table 1. As observed, doping process decreases the charge transfer resistance, which is indicative of an increase in carrier transfer rate between the sample and electrolyte. Therefore, $Fe_2 + N_{10}/TiO_2$ can promote the electron transport rate in photocatalytic reactions.

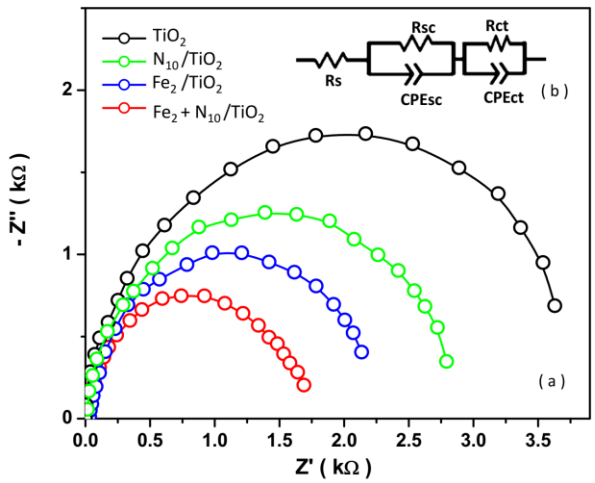

Figure 3. (a) Nyquist curves of the TiO_2, Fe_2/TiO_2, N_{10}/TiO_2, and $Fe_2 + N_{10}/TiO_2$ modified GCE, and (b) the equivalent circuit.

Table 2. Fitted parameters of the Nyquist plots for the TiO_2, Fe_2/TiO_2, N_{10}/TiO_2, and $Fe_2 + N_{10}/TiO_2$

Sample	Rs (Ω)	Rsc (Ω)	CPEsc		Rct (Ω)	CPEct	
			Q (mFs^{n-1})	n		Q (mFs^{n-1})	n
TiO_2	3.09	393.03	1.71	0.75	3380.1	0.32	0.97
Fe_2/TiO_2	4.61	1.61	0.41	0.63	2439.8	0.15	0.93
N_{10}/TiO_2	1.69	0.38	3.31	0.66	2279.2	0.81	0.91
$Fe_2 + N_{10}/TiO_2$	1.78	0.12	3.17	0.87	1620.1	1.07	0.96

3.3. Optical analysis

The UV–vis absorption spectra of pure and doped TiO_2 samples are presented in Figure 4. Generally, the pure crystalline TiO_2 exhibits a strong band-edge wavelength of below 403 nm. After doping with N and F, the absorption band-edge wavelength of Fe_2/TiO_2, N_{10}/TiO_2, and $Fe_2 + N_{10}/TiO_2$ are red-shifted to 416, 447 and 467 nm, respectively. The optical band gap (E_g) from the UV–vis absorption spectra can be calculated using the following formula [47, 48]:

$$E_g = 1240/\lambda \quad (3)$$

where λ is the absorption band-edge wavelength. The E_g of pure TiO_2, Fe_2/TiO_2, N_{10}/TiO_2, and $Fe_2 + N_{10}/TiO_2$ are obtained at 3.07, 2.98, 2.77 and 2.65 eV, respectively, indicating that the doping leads to a narrowing of the E_g and red-shifting of absorption towards the visible-light region. These results confirm that the sol-gel synthesis and doping of Fe and N lead to enhancement of the absorption towards the visible region which is attributed to the replacement of N atoms in portion of O atoms of TiO_2 crystal, and localization of N_2p states in the band structure in the form of substitutional and interstitial N states. It corresponds the formation of a new energy level on top of the valance band of TiO_2 and narrow band gap, and the enhancement of photocatalytic activity in the visible range [49-51]. Moreover, it has been reported that metal doping can form the new energy level within the band gap of TiO_2, implying that electron can be excited from the defect state to the TiO_2 conduction band at lower photon energies than in the UV region [52, 53]. The red-shifted of absorption edge in a semiconductor can be associated with the charge-transfer transition between the orbital d electrons of Fe and the TiO_2 conduction or valance band [54]. It can result in the generation of electron-hole pairs and an improvement in the visible light response of TiO_2-based photocatalyst [52, 54, 55]. In addition, it can be clearly observed that further lowering of the E_g and red-shifting are observed for $Fe_2 + N_{10}/TiO_2$ sample. It is related to the synergistic effect of both Fe and N in the $Fe_2 + N_{10}/TiO_2$ nanoparticles.

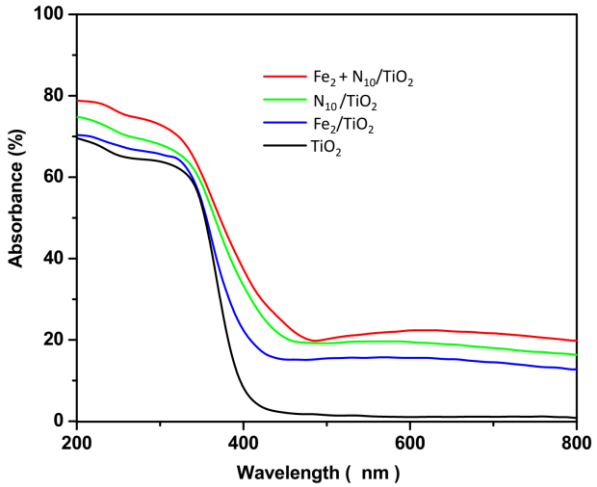

Figure 4. UV–vis absorption spectra of pure TiO_2 and doped TiO_2.

3.4. Photocatalytic degradation studies

Figure 5 shows the photodegradation of 100 ml of 5 mg/l o-CP aqueous solution by pure and doped TiO_2 under simulated sunlight irradiation. For more comparison, the results of photodegradation in the dark (first 45 minutes) and a blank sample (without photocatalyst) are also displayed in Figure 5. It is demonstrated to have less than 1% degradation efficiency for all samples in the dark after 45 minutes. Comparison between the degradation in light and darkness reveals the great effect of simulated sunlight on the removal of o-CP from water. The degradation blank sample also shows less than 2.5% degradation efficiency after 180 minutes irradiation of light, indicating its negligible value toward the photodegradation in the presence of photocatalysts, indicating the remarkable effect of pure and doped TiO_2 on the degradation of the o-CP under simulated sunlight irradiation. After 120 minutes of irradiation, the complete degradation efficiency of o-CP is obtained Fe_2+N_{10}/TiO_2, and after 180 minutes of irradiation, the degradation efficiency of o-CP is obtained as 60.1, 70.3 and 90.2 % for pure TiO_2 and Fe_2–TiO_2 and N_{10}– TiO_2, respectively. Accordingly, Fe and N co-doping promote the photocatalytic activity of TiO_2 due to the synergistic effects of both Fe and N in TiO_2 structure and improvement of electron trapping to prevent electron-hole recombination during irradiation, demonstrating enhanced photoactivity. Furthermore, the formation of Schottky barrier at the metal-semiconductor interface with the generation an electron depletion layer at the Fe/TiO_2 junction leads to the downward bending of TiO_2 energy bands [56]. Fe dopants serve as passive electron sinks and act as a trapping center for photogenerated electrons and hole pairs because photogenerated electrons are readily transferred through the heterojunction barrier and photogenerated holes are directed towards the interface [57, 58]. Therefore, it may promote separation rate and the photogenerated carrier's lifetime [56, 57]. As a consequence, the photodegradation rate is improved.

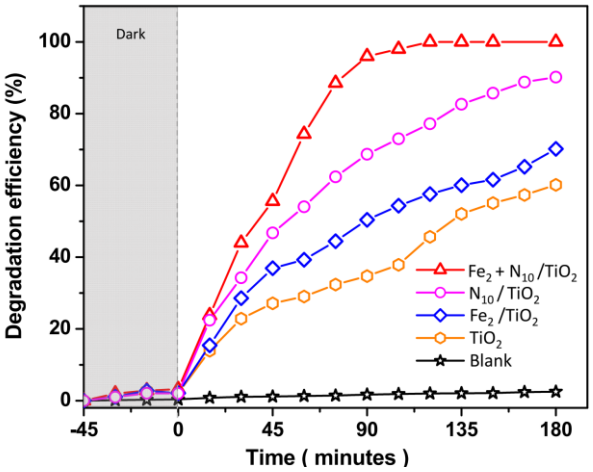

Figure 5. Photodegradation of 100 ml of 5 mg/l o-CP aqueous solution by of pure and doped TiO_2 in dark and under simulated sunlight irradiation

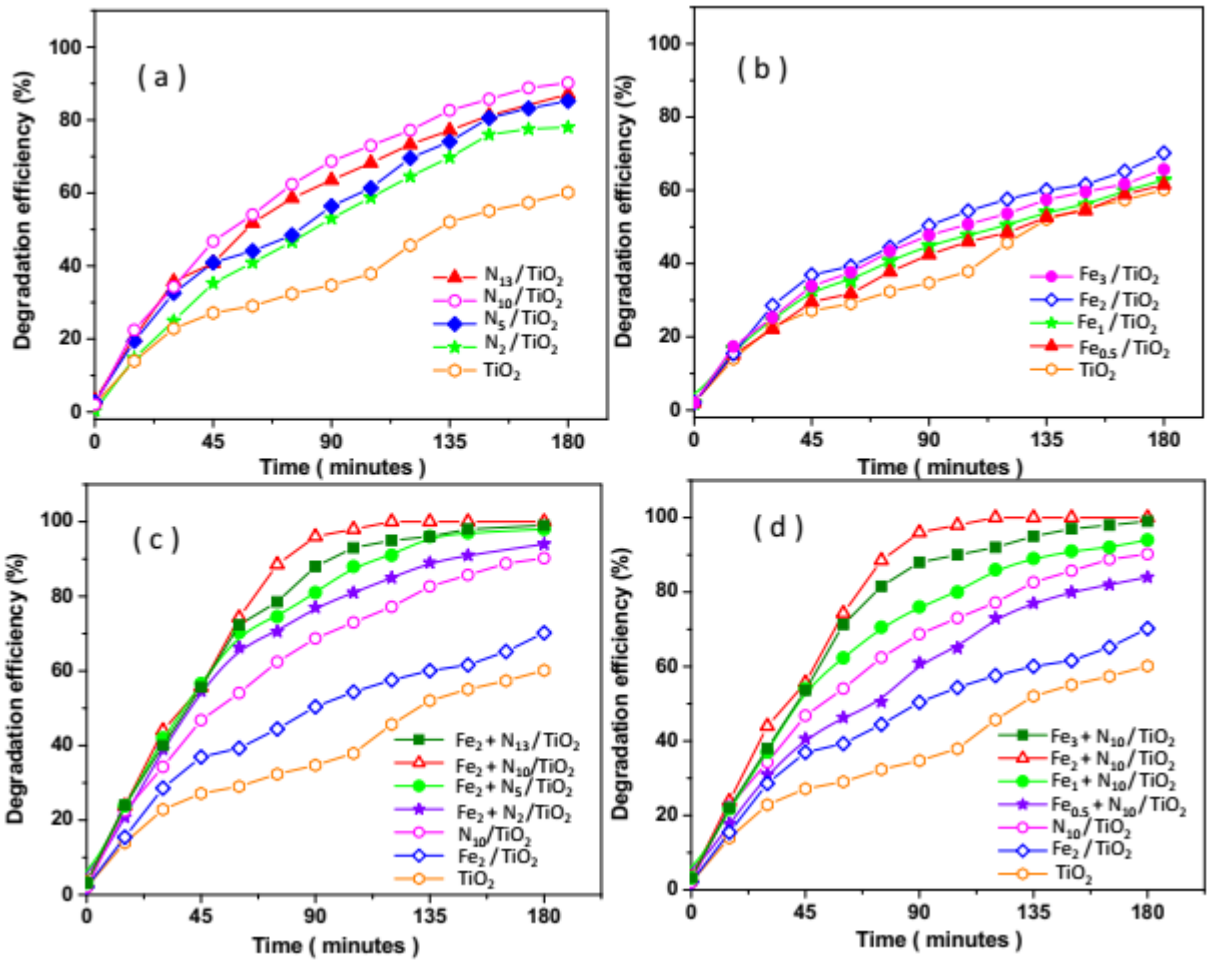

Figure 6. The photodegradation of 100 ml of 5 mg/l o-CP aqueous solution under simulated sunlight irradiation using Fe_y+N_x/TiO_2 with different N amount (a and c) and different Fe amount (b and d) under simulated sunlight irradiation

In order to obtain the optimal amounts of N and Fe dopants in co-doped TiO_2, the photodegradation performance of doped and co-doped TiO_2 ($Fe_y + N_x/TiO_2$; y = 0.5, 1, 2 and 3 %, and x = 2, 5, 10 and 13 %) was compared with pure TiO_2, N doped TiO_2 (N_{10}/TiO_2) and Fe doped TiO_2 (Fe_2/TiO_2). Figures 6a and 6c show the photodegradation of 100 ml of 5 mg/l o-CP aqueous solution using N_x/TiO_2 and Fe_2+N_x/TiO_2 with different N amounts (x = 2, 5, 10 and 13 %). It is clearly observed that the photocatalytic performance of N doped and TiO_2 Fe+N co-doped TiO_2 increases with the increase of N dopant amount from 2% to 10%, whereas it decreases slightly when N dopant reaches 13% due to an excessive amount of N, which corresponds to increasing the N dopant amount [59, 60]. It results in the increase of oxygen vacancy and Ti^{3+} that it not only corresponds to a rise of photocatalytic activity but also forms some oxygen vacancy and Ti^{3+} sites in an excessive amount of N which can act as the recombination centers of photo-induced carriers, leading to a decrease in photocatalytic activity [60].

Figures 6b and 6d demonstrate the effect of Fe amount on the photocatalytic activity of Fe_y/TiO_2 and Fe_y+N_{10}/TiO_2 (y = 0.5, 1, 2 and 3 %) for the photodegradation of 100 ml of 5 mg/l o-CP aqueous solution. It can be found that the degradation efficiency of o-CP can reach a maximum for Fe loading amount of 2% in Fe_2, N_{10} codoped TiO_2, implying the significant ability to transfer both electrons and holes and effective trap of photo-induced electrons because of trap states of defects and strong electron-withdrawing ability of metallic Fe [61]. Whereas, excessive Fe amount as dopant in Fe_y+N_{10}/TiO_2 (more than 2%) decrease the photocatalytic activity due to the increase in oxygen vacancy which acts as an electron-hole recombination center [62-64], and light penetration can be limited due to light absorption and scattering by the dopant centers in catalyst [65]. Therefore, Fe_2+N_{10}/TiO_2 shows the best photodegradation rate for removal of o-CP, and the optimal content of Fe dopant in the Fe_y+N_{10}/TiO_2 is 2%.

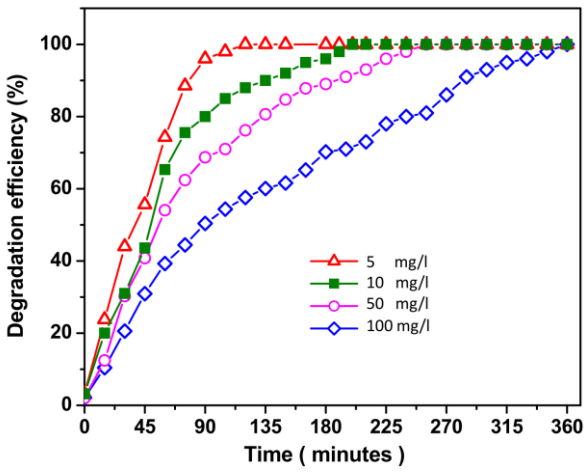

Figure 7. Effect of initial concentration of o-CP on photocatalytic activity of Fe_2+N_{10}/TiO_2 under simulated sunlight irradiation

Figure 7 depicts the effect of the initial concentration of o-CP on the photocatalytic activity of Fe_2+N_{10}/TiO_2. As illustrated, the complete removal of 5, 10, 50 and 100 mg/l of o-CP is obtained after

120, 200, 255 and 360 minutes of simulated sunlight irradiation, respectively. In fixed catalyst dosage, the photodegradation rate is decreased with the increase of the o-CP initial concentration of o-CP, which can be associated with an insufficient concentration of reactive oxygen species produced during the photocatalytic process and the absorption of more o-CP molecules on the catalyst surface [66].

The photocatalytic activity of Fe_2+N_{10}/TiO_2 for photodegradation of o-CP is compared with the photocatalytic performance of reported systems in the literature, and the results are summarized in Table 1. As observed, Fe_2+N_{10}/TiO_2 shows effective performance for photodegradation of o-CP under simulated sunlight because of the synergistic effect of both Fe and N in the Fe_2+N_{10}/TiO_2 nanoparticles that lead to a decrease the recombination rate of photogenerated carries and a narrowing band gap. The results demonstrate the feasibility and novelty of photocatalytic treatment of o-CP using a Fe_2+N_{10}/TiO_2 photocatalyst, including the simple preparation of a low-cost conducting photocatalyst and the evaluation of the synergistic effect of Fe and N dopants in co-doped TiO_2 as an effective photocatalyst for fast photodegradation of o-CP under simulated sunlight.

Table 1. Comparison of photocatalytic performance of Fe_2+N_{10}/TiO_2 with the reported systems in the literatures for photodegradation of o-CP

Photocatalyst	o-CP content (mg/l)	Light source	Degradation time (minute)	Degradation efficiency (%)	Ref.
Fe_2+N_{10}/TiO_2	100	Simulated sunlight	360	100	This work
	50		255		
	10		200		
	5		120		
Fly ash/TiO_2	50	UV	180	98.9	[26]
TiO_2	50	UV	180	78.7	[26]
Cu/Cl-g-C_3N_4	10	Visible	60	48.7	[27]
TiO_2/NiO-rGO	100	Visible	480	88.4	[28]
Ag-TiO_2/$H_3PW_{12}O_{40}$	5	UV	240	82.40	[30]
ZnO	60	UV	90	100	[29]
$H_3PW_{12}O_{40}$/graphene/TiO_2	5	Simulated sunlight	300	97.02	[31]
TiO_2	10	UV	90	100	[32]

4. CONCLUSION

This work presents the synthesis of nanostructured photocatalyst $Fe_y + N_x/TiO_2$ (y = 0.5, 1, 2 and 3 %, and x = 2, 5, 10 and 13 %) for degradation of o-CP in water. The Fe, N co-doped TiO_2 was prepared using the sol-gel method. The results of crystallographic and morphological analyses showed the successful synthesis and doping of TiO_2 with Fe, N and Fe-N. Results of EIS study illustrated that the doping process in Fe_y+N_x/TiO_2 decreased the charge transfer resistance and increased of carrier transfer rate between sample and electrolyte. The results of the analysis of UV–vis absorption spectra revealed that the E_g of pure TiO_2, Fe_2/TiO_2, N_{10}/TiO_2, and $Fe_2 + N_{10}/TiO_2$ were obtained at 3.07, 2.98,

2.77 and 2.65 eV, respectively, indicating that the doping leads to a narrowing of the E_g. Photodegradation studies of $Fe_y+ N_x/TiO_2$ showed that Fe_2+N_{10}/TiO_2 had the optimal content of Fe and N dopants for fast degradation o-CP aqueous solution. The 100% degradation of 5, 10, 50 and 100 mg/l of o-CP was obtained after 120, 200, 255 and 360 minutes of simulated sunlight irradiation, respectively. The effective photodegradation of o-CP under simulated sunlight was attributed to the synergistic effect of both Fe and N in the Fe_2+N_{10}/TiO_2 nanoparticles.

References

1. S. Li, Y. Tian, Q. Ding and W. Liu, *Chemosphere*, 94 (2014) 164.
2. S.-S. Yang, X.-L. Yu, M.-Q. Ding, L. He, G.-L. Cao, L. Zhao, Y. Tao, J.-W. Pang, S.-W. Bai and J. Ding, *Water Research*, 189 (2021) 116576.
3. M.T. Sultan, H.S. Al-Lami and A.H. Al-Dujiali, *Desalination and Water Treatment*, 150 (2019) 192.
4. G. Li, S. Huang, N. Zhu, H. Yuan, D. Ge and Y. Wei, *Chemical Engineering Journal*, 421 (2021) 127852.
5. L. He, M.-X. Li, F. Chen, S.-S. Yang, J. Ding, L. Ding and N.-Q. Ren, *Journal of Hazardous Materials*, 417 (2021) 126113.
6. A. Hammam, M.S. Zaki, R.A. Yousef and O. Fawzi, *Advances in environmental biology*, 9 (2015) 38.
7. H. Liu, X.-X. Li, X.-Y. Liu, Z.-H. Ma, Z.-Y. Yin, W.-W. Yang and Y.-S. Yu, *Rare Metals*, 40 (2021) 808.
8. C. Zhao, M. Xi, J. Huo and C. He, *Physical Chemistry Chemical Physics*, 23 (2021) 23219.
9. J.-Z. Cheng, Z.-R. Tan, Y.-Q. Xing, Z.-Q. Shen, Y.-J. Zhang, L.-L. Liu, K. Yang, L. Chen and S.-Y. Liu, *Journal of Materials Chemistry A*, 9 (2021) 5787.
10. R. Wang, C. He, W. Chen, L. Fu, C. Zhao, J. Huo and C. Sun, *Nanoscale*, 13 (2021) 19247.
11. A. Baradaran-Rafii, M. Akbari, E. Shirzadeh and M. Shams, *Journal of ophthalmic & vision research*, 10 (2015) 90.
12. A. Medghalchi, M. Akbari, Y. Alizadeh and R.S. Moghadam, *Journal of current ophthalmology*, 30 (2018) 353.
13. Y. Zheng, Y. Guo, L. Luo and T. Zhu, *Catalysts*, 8 (2018) 37.
14. M. Xi, X. Fu, H. Yang, C. He, L. Fu, X. Cheng and J. Guo, *Chinese Chemical Letters*, (2021)
15. D. Xu and H. Ma, *Journal of Cleaner Production*, 313 (2021) 127758.
16. X. Zhang, Y. Tang, F. Zhang and C.S. Lee, *Advanced Energy Materials*, 6 (2016) 1502588.
17. M. Khosravi, *Open Access Macedonian Journal of Medical Sciences*, 8 (2020) 553.
18. H. Maleh, M. Alizadeh, F. Karimi, M. Baghayeri, L. Fu, J. Rouhi, C. Karaman, O. Karaman and R. Boukherroub, *Chemosphere*, (2021) 132928.
19. N. Rao, A. Dubey, S. Mohanty, P. Khare, R. Jain and S. Kaul, *Journal of hazardous materials*, 101 (2003) 301.
20. G. Li, S. Huang, N. Zhu, H. Yuan and D. Ge, *Journal of Hazardous Materials*, 403 (2021) 123981.
21. T. Sankara Narayanan, G. Magesh and N. Rajendran, *Fresenius Environmental Bulletin*, 12 (2003) 776.
22. G. Jin-zhang, Y. Wu, L. Yong-jun, C. Ping, N. Peng-jun and L. Quan-fang, *Plasma Science and Technology*, 5 (2003) 1609.
23. J. Huo, L. Fu, C. Zhao and C. He, *Chinese Chemical Letters*, 32 (2021) 2269.
24. W. BIAN, M. ZHOU and L. LEI, *Journal of Chemical Industry and Engineering (China)*, 1 (2005) 1.

25. S.A. Boyd, D.R. Shelton, D. Berry and J.M. Tiedje, *Applied and Environmental Microbiology*, 46 (1983) 50.
26. M. Malakootian, A. Mesdaghinia and S. Rezaei, *Journal of Kerman University of Medical Sciences*, 24 (2017) 147.
27. C. Li, S. Yu, X. Zhang, Y. Wang, C. Liu, G. Chen and H. Dong, *Journal of colloid and interface science*, 538 (2019) 462.
28. A. Sharma and B.-K. Lee, *Journal of environmental management*, 181 (2016) 563.
29. S. Lathasree, A.N. Rao, B. SivaSankar, V. Sadasivam and K. Rengaraj, *Journal of Molecular Catalysis A: Chemical*, 223 (2004) 101.
30. N. Lu, Y. Wang, S. Ning, W. Zhao, M. Qian, Y. Ma, J. Wang, L. Fan, J. Guan and X. Yuan, *Scientific Reports*, 7 (2017) 17298.
31. Y. Ma, Y. Zhang, X. Zhu, N. Lu, C. Li, X. Yuan and J. Qu, *Environmental Research*, 188 (2020) 109786.
32. G. Sivalingam, M. Priya and G. Madras, *Applied Catalysis B: Environmental*, 51 (2004) 67.
33. L. He, C. Yang, J. Ding, M.-Y. Lu, C.-X. Chen, G.-Y. Wang, J.-Q. Jiang, L. Ding, G.-S. Liu and N.-Q. Ren, *Applied Catalysis B: Environmental*, 303 (2022) 120880.
34. R. Rezapour-Nasrabad, *International Journal of Pharmaceutical Research*, 11 (2019) 1.
35. Y. Orooji, B. Tanhaei, A. Ayati, S.H. Tabrizi, M. Alizadeh, F.F. Bamoharram, F. Karimi, S. Salmanpour, J. Rouhi and S. Afshar, *Chemosphere*, 281 (2021) 130795.
36. C.G. Aba-Guevara, I.E. Medina-Ramírez, A. Hernández-Ramírez, J. Jáuregui-Rincón, J.A. Lozano-Álvarez and J.L. Rodríguez-López, *Ceramics International*, 43 (2017) 5068.
37. C.M. Malengreaux, S.L. Pirard, G. Léonard, J.G. Mahy, M. Herlitschke, B. Klobes, R. Hermann, B. Heinrichs and J.R. Bartlett, *Journal of alloys and compounds*, 691 (2017) 726.
38. A. Rajamani, R. Kannan, S. Krishnan, S. Ramakrishnan, S.M. Raj, D. Kumaresan, N. Kothurkar and M. Rangarajan, *Journal of nanoscience and nanotechnology*, 15 (2015) 5042.
39. S.H. Othman, S. Abdul Rashid, T.I. Mohd Ghazi and N. Abdullah, *Journal of Nanomaterials*, 2011 (2011) 1.
40. S.S. Gargari, R. Fateh, M. Bakhshali-Bakhtiari, M. Saleh, M. Mirzamoradi and M. Bakhtiyari, *BMC pregnancy and childbirth*, 20 (2020) 1.
41. K. Li, H. Wang, C. Pan, J. Wei, R. Xiong and J. Shi, *International Journal of Photoenergy*, 2012 (2012) 1.
42. J. Yu, M. Zhou, H. Yu, Q. Zhang and Y. Yu, *Materials Chemistry and Physics*, 95 (2006) 193.
43. H. Zhang, D. Gu, L. Xi, H. Zhang, M. Xia and C. Ma, *Journal of Materials Science & Technology*, 35 (2019) 1128.
44. Y.-H. Chiu, T.-H. Lai, C.-Y. Chen, P.-Y. Hsieh, K. Ozasa, M. Niinomi, K. Okada, T.-F.M. Chang, N. Matsushita and M. Sone, *ACS applied materials & interfaces*, 10 (2018) 22997.
45. Y. Li, *International Journal of Electrochemical Science*, 17 (2022) 22014.
46. H. Sun, D. Qin, S. Huang, X. Guo, D. Li, Y. Luo and Q. Meng, *Energy & Environmental Science*, 4 (2011) 2630.
47. Y. Lu, R. Jin, Y. Qiao, W. Liu, K. Wang, X. Wang and C. Wang, *International Journal of Electrochemical Science*, 15 (2020) 10243.
48. W. Qin, J. Qi, Y. Chen, H. Li and X. Wu, *International Journal of Electrochemical Science*, 8 (2013) 7680.
49. X. Cheng, X. Yu, Z. Xing and J. Wan, *Energy Procedia*, 16 (2012) 598.
50. R. Jaiswal, N. Patel, D. Kothari and A. Miotello, *Applied Catalysis B: Environmental*, 126 (2012) 47.
51. R. Hassanzadeh, A. Siabi-Garjan, H. Savaloni and R. Savari, *Materials Research Express*, 6 (2019) 106429.
52. A. Zaleska, *Recent patents on engineering*, 2 (2008) 157.

53. M. Mirzamoradi, F. Hasani Nejhad, R. Jamali, Z. Heidar and M. Bakhtiyari, *The Journal of Maternal-Fetal & Neonatal Medicine*, 33 (2020) 2533.
54. S. George, S. Pokhrel, Z. Ji, B.L. Henderson, T. Xia, L. Li, J.I. Zink, A.E. Nel and L. Mädler, *Journal of the American Chemical Society*, 133 (2011) 11270.
55. S. Banerjee, S.C. Pillai, P. Falaras, K.E. O'shea, J.A. Byrne and D.D. Dionysiou, *The journal of physical chemistry letters*, 5 (2014) 2543.
56. L.G. Devi and R. Kavitha, *Applied Surface Science*, 360 (2016) 601.
57. M. Ismael, *Journal of Environmental Chemical Engineering*, 8 (2020) 103676.
58. H. Rahimi and P. Karimian, *Journal of Critical Reviews*, 7 (2020) 284.
59. K. Prabakar, T. Takahashi, T. Nezuka, K. Takahashi, T. Nakashima, Y. Kubota and A. Fujishima, *Renewable Energy*, 33 (2008) 277.
60. X. Cheng, X. Yu, Z. Xing and L. Yang, *Arabian Journal of Chemistry*, 9 (2016) S1706.
61. B. Li, S. Wu and X. Gao, *Nanotechnology Reviews*, 9 (2020) 1080.
62. Y. Castro, N. Arconada and A. Durán, *Boletín de la Sociedad Española de Cerámica y Vidrio*, 54 (2015) 11.
63. M.J. Valero-Romero, J.G. Santaclara, L. Oar-Arteta, L. van Koppen, D.Y. Osadchii, J. Gascon and F. Kapteijn, *Chemical Engineering Journal*, 360 (2019) 75.
64. H. Zhang, C. Liang, J. Liu, Z. Tian, G. Wang and W. Cai, *Langmuir*, 28 (2012) 3938.
65. I. Horovitz, D. Avisar, M.A. Baker, R. Grilli, L. Lozzi, D. Di Camillo and H. Mamane, *Journal of hazardous materials*, 310 (2016) 98.
66. E.S. Elmolla and M. Chaudhuri, *Desalination*, 252 (2010) 46.